Int. J. Heat Mass Transfer. Vol. 36, No. 7, pp. 1749–1762, 1993
Printed in Great Britain

0017-9310/93 $6.00 + 0.00
Pergamon Press Ltd

Infrared gas radiation from a homogeneously turbulent medium

F. KRITZSTEIN and A. SOUFIANI

Laboratoire d'Energétique Moléculaire et Macroscopique, Combustion, du CNRS et de l'ECP, Ecole Centrale Paris, Grande Voie des Vignes, 92295 Chatenay-Malabry, France

(*Received for publication* 6 *November* 1992)

Abstract—Mean infrared radiation from a turbulent, statistically uniform medium is studied theoretically. A stochastic approach is used in which instantaneous temperature and concentration fluctuations are generated by Fourier transforming various forms of the space–time correlation function. The effect of the shape of the spatial correlation function on the model results is found to be negligible. We discuss first the influence of the spectroscopic parameters of an isolated Lorentz line on mean radiative intensities. It is shown that the effects of turbulence depend strongly on the energy of the lower level of the transition. Statistical narrow-band calculations are then carried out for four CO_2 and four H_2O bands. The contribution of turbulence to the mean band-integrated radiative intensity is generally greater when the hot emitting medium is viewed through a cold absorbing one. The influence of turbulence integral length-scale, optical thickness of the medium and band locations are discussed. It is also found that the turbulence contribution to the radiative intensity, when integrated over the entire infrared spectrum, decreases quickly when the mean temperture increases in the range [800–2000 K]. In the case of combined temperature and concentration fluctuations, positive cross-correlations lead to an increase in the tubulence contribution due to temperature fluctuations alone, while negative cross-correlations lead to a decrease in this contribution.

1. INTRODUCTION

IN APPLICATIONS where infrared gas radiation is the predominant heat transfer mode, flows of gaseous mixtures are generally in the turbulent flow regime. Large flames encountered in accidental fires or offshore oil and gas facilities, rocket and aircraft combustion chambers including the hot jets from these chambers are some typical examples. The prediction of such flows is most often based on a closure model which leads to the mean temperature $\bar{T}$ and molar fraction $\bar{x}_j$ fields, and in some cases, the mean square fields $\overline{T'^2}$ and $\overline{x_j'^2}$ as well.

Two kinds of radiation/turbulence interactions are recognized. The first is related to the influence of molecular and particle radiation on the properties of thermal turbulence [1–3]. It has been shown that radiative transfer acts as a dissipative process for large thermal eddies and tends to smooth temperature fluctuations. These effects are particularly relevant when turbulence dissipation due to molecular diffusion is small compared to the radiative dissipation (e.g. atmospheric applications) and will not be considered in this study.

The second interaction is related to the effects of temperature and molar fraction fluctuations on the mean radiative flux from the hot turbulent mixture. Several studies have shown that mean radiative quantities may differ significantly from those based on the mean temperature and concentration fields. This is the result of the strong nonlinearities in the relationship between radiation and the instantaneous scalar fields. The quasi-exponential dependence of the blackbody intensity with temperature in the Wien region of the spectrum is an example of these nonlinearities. Turbulence effects in practical situations may be very important since fluctuation intensities can reach values as high as 40% in flames [4, 5].

Faeth and coworkers have studied the infrared radiation from various turbulent flames with different fuels, for both luminous and nonluminous flames [6–14]. Their theoretical predictions are based on a k–ε–g turbulence model for the calculation of the nonhomogeneous flowfield and flame structure, and the use of laminar flamelet state relationships between instantaneous mixture fraction and scalar properties. Stochastic simulations are used to predict mean and fluctuating radiative intensities along several paths in the flame. Gaseous radiation is computed from a statistical narrow-band model, while soot radiation is considered in the Rayleigh limit. In the earlier studies [6–10], the emitting gaseous column is divided into statistically independent homogeneous and isothermal columns having lengths equal to the local dissipation or integral length-scale and this treatment ignores the existence of spatial correlations. In more recent papers [11–14], spatial and temporal correlations are considered in order to analyse the fluctuations of radiative intensities at some specified wavelengths. The results of these studies show that spectral intensities may be increased by up to a factor of three when turbulence/radiation interactions are taken into account. Measured radiative intensities generally fell between the predictions from mean scalar properties and those from the stochastic analysis.

For similar applications, Cox [4] uses the gray gas

NOMENCLATURE

$C_x(r)$ two-point/one-time autocorrelation function (ensemble average)
$C_t(\tau)$ one-point/two-time autocorrelation function (ensemble average)
$C(r,\tau)$ two-point/two-time autocorrelation function (ensemble average)
E'' energy of the lower level of a transition
I radiative intensity integrated over a line, a band or the spectrum
I_ν spectral radiative intensity
I_ν^b blackbody spectral intensity
k_i turbulence discrete wave number
$\bar{k}$ mean line intensity to mean line spacing ratio inside $\Delta\nu$
L_x length of the hot radiating column
M total number of discrete spatial points
N total number of time intervals
p total pressure
$Q(T)$ rovibrational partition function
r separation variable in two-point correlation functions
t_c turbulence integral time-scale
$R_{x_a T}$ two-point molar fraction–temperature correlation function
$S(T)$ absorption line strength
t_0 time observation
t time
T_0 mean absolute temperature
$T'(x,t)$ temperature fluctuation
u optical thickness at line center
w_i discrete frequency of turbulence
x abscissa along the transfer direction
x_a molar fraction of the absorbing species
x'_a, x'_j molar fraction fluctuation.

Greek symbols
$\alpha(t)$ uniform random number
$\gamma(T)$ Lorentz line half-width at half-maximum
$\bar{\gamma}$ mean line half-width inside $\Delta\nu$
$\Delta\nu$ narrow-band model spectral range
δ mean line spacing inside $\Delta\nu$
θ r.m.s. value of temperature fluctuations
κ_ν spectral absorption coefficient
Λ turbulence integral length-scale
ν radiation wave number
σ r.m.s. value of molar fraction fluctuations
τ separation variable in two-time correlation functions
$\tau_{\Delta\nu}$ transmissivity averaged over $\Delta\nu$
φ_i phase corresponding to k_i.

Symbols
$\hat{\Phi}$ Fourier transform
$\bar{\Phi}^t$ time averaging
$\langle\Phi\rangle$ ensemble averaging.

Subscripts
m, i discrete spatial position
n, j, l discrete time.

approximation and obtains the mean radiative fluxes from a Taylor expansion of the product $\varepsilon\overline{T^4}$, where ε is the gas emissivity. This study shows that high order terms in the expansion may be predominant in practical situations.

For an application involving the long range detection of an axisymmetric missile exhaust plume, Pearce and Varma studied turbulence/radiation interactions in the band wings of the 4.3 μm CO_2 band [15]. They used second order Taylor expansions of the blackbody intensity and the monochromatic absorption coefficient, because their turbulence intensities were relatively small. They considered first the case of an isolated spectral line and showed the strong sensitivity of the line shape and the integrated intensity to the energy E'' of the lower level of the vibrational–rotational transition. Bandpass calculations were then carried out by using line by line computations for several paths through the plume. They found that radiance augmentation due to turbulence depends strongly on the region considered in the flowfield.

Turbulence/radiation interactions have also been studied for the case of gaseous internal flows in order to predict wall–gas radiative fluxes. Song and Viskanta have investigated the case of a turbulent flame inside a two-dimensional furnace [16]. They invoked simplifying assumptions concerning correlation functions and gaseous radiative properties and solved the fully coupled reacting flow and radiation problem. Their results show that temperature and concentration fluctuations lead to an increase in radiative fluxes (up to about 80%) when the flame occupies a large volume fraction of the combustion system. In a related study, Soufiani *et al.* investigated these interactions in the case of a turbulent channel flow of radiating but nonreacting gas [17]. They found that temperature fluctuation effects on mean wall radiative fluxes are limited to about 10% in these flows, since fluctuation intensities, produced mainly by mean velocity and temperature gradients, are small in comparison with those encountered in reacting turbulent flows.

Finally, it is worth noting the studies of Daily [18] and Charpenel [19] which are related to the effects of turbulence on optical measurements of temperature and concentration when using absorption or emission techniques.

In the present paper, a theoretical study concerning

the interaction between turbulence and radiation in the case of homogeneous and isotropic turbulence is presented. Parametric studies in this simple case allow us to gain insight on the most relevant parameters affecting this phenomenon. Attention is focused on the physical representation of both turbulence statistical properties and real molecular radiative spectra. We use a stochastic approach in which the instantaneous temperature and concentration fluctuations are generated from spatio–temporal correlation functions (Section 2). Results from different analytical forms of the correlation function are compared. In Sections 3 and 4, we consider the effects of temperature fluctuations alone. Radiation from an isolated spectral line is studied in Section 3 in order to point out the influence of spectroscopic parameters. The results from this section are useful both for the analysis of low spectral resolution results and for the application to optical diagnostics through turbulent media. Section 4 is related to molecular bands of H_2O and CO_2. A statistical narrow-band model, associated with the Curtis–Godson approximation is used. In this section a distinction between the case of radiation directly from a statistically homogeneous hot medium and the case of radiation emitted by this medium and transmitted through a cold atmospheric medium is made. Finally, the combined effects of temperature and molar fraction fluctuations are considered in Section 5.

2. INSTANTANEOUS SCALAR FIELDS

The mean radiative flux incident on a detector can be obtained from the mean incident intensity by integrating over all the propagation directions. In this study, we consider the effects of turbulence on radiative intensity in a particular direction Ox, without specifying the entire geometry of the system. The intersection of this direction with the emitting medium defines a gaseous column of length L_x over which spatial and temporal variations of temperature and molar fractions are to be specified.

General method

The scalar fields are assumed to be stationary, homogeneous stochastic processes, with a Gaussian probability density function. They are determined from these assumptions and the following properties:

$$\langle T'(x,t)\rangle = 0, \tag{1}$$

$$\langle T'(x,t)T'(x+r,t+\tau)\rangle = \theta^2 C(r,\tau), \tag{2}$$

where $T'(x,t)$ is the temperature or molar fraction fluctuation around the mean value T_0, and the angle brackets denote an average over the ensemble of realizations. $C(r,\tau)$ is the space–time correlation function satisfying $C(0,0)=1$, and θ is the r.m.s. value of the scalar fluctuation. The choice of the functional form of $C(r,\tau)$ is discussed below. As the function $T'(x,t)$ is to be defined only in the range $0 \leqslant x \leqslant L_x$ and for a finite time interval $0 \leqslant t \leqslant t_0$, we assume that it is a periodic function with periods L_x and t_0. The manner in which $T'(x,t)$ is generated numerically from the above properties is an extension of the approach given in ref. [20] for space and time varying processes and is described in Appendix A. For the discrete values $x_m = m\Delta x$ and $t_n = n\Delta t$, the result is

$$T'(x_m,t_n) = \theta \sum_{k=-M}^{M-1}\sum_{w=-N}^{N-1} \frac{1}{2}\frac{1}{\sqrt{L_x}}\frac{1}{\sqrt{t_0}} \times (A_{k,w}+\mathrm{i}B_{k,w})\hat{C}^{1/2}\left(\frac{2\pi k}{L_x},\frac{2\pi w}{t_0}\right)\mathrm{e}^{2\mathrm{i}\pi(mk/2M+nw/2N)}. \tag{3}$$

In this equation, M and N are such that $L_x = 2M\Delta x$ and $t_0 = 2N\Delta t$. $2\pi k/L_x$ and $2\pi w/t_0$ are discrete values of the turbulent wave number and frequency, respectively. $\hat{C}$ is the two-dimensional Fourier transform of $C(r,\tau)$. $A_{k,w}$ and $B_{k,w}$ are independent, random, Gaussian variables with zero mean and a standard deviation of unity. They satisfy the conditions $A_{k,w} = A_{-k,-w}$ and $B_{k,w} = -B_{-k,-w}$ in order to yield real values of $T'(x,t)$.

Up to this point, we are able to generate different transient turbulent fields by assigning to each field a given set of random variables $A_{k,w}$ and $B_{k,w}$. With the assumption that the stochastic process is ergodic, ensemble averaging is equivalent to time averaging. We then consider only one transient field from which mean radiative intensities are computed by time averaging. In practice, two sets of $2MN$ Gaussian random variables are generated ($A_{k,w}$ and $B_{k,w}$), and the inverse discrete Fourier transform of

$$(A_{k,w}+\mathrm{i}B_{k,w})\left[\hat{C}^{1/2}\left(\frac{2\pi k}{L_x},\frac{2\pi w}{t_0}\right)\right]$$

is carried out by using a FFT algorithm. The stochastic simulation of radiative transfer is achieved through time iterations where instantaneous radiative intensities are computed for each t_n, and then averaged until a convergent solution is reached. In this way the use of a space–time correlation function enables the statistical description of temporal variations of the emitted intensity, even if we are mostly interested in mean values.

For computational considerations, the maximum wave number $2\pi M/L_x$ is chosen such that

$$\frac{\hat{C}\left(\frac{2\pi M}{L_x},\frac{2\pi w}{t_0}\right)}{\hat{C}\left(\frac{2\pi}{L_x},\frac{2\pi w}{t_0}\right)} \leqslant 0.01 \text{ for any } w$$

in order to account for the smallest eddies which contribute to the energy power spectrum of $T'(x,t)$. The required number of time realizations for convergence depends on the ratio Λ/L_x (where Λ is the integral length-scale of turbulence) and on the optical thickness of the largest eddies. For integral length-scales which are very small in comparison with the column

length, practically all the allowed variations of $T'(x,t)$ are found in one spatial distribution. Radiative intensity is then independent of time (as found by Cox [4]), provided that the large eddies are not optically thick. But in the case of $\Lambda/L_x = 1$ for instance, about 10 000 samples are generally required for a convergence better than 2%. On the other hand, when the instantaneous value of $T_0 + T'(x,t)$ is negative, it is set numerically to a minimum value (100 K for temperature and 0 for molar fraction). The number of pairs (x_m, t_n) for which this occurs is sufficiently small, and this procedure does not modify appreciably the statistical properties of the field.

The procedure described above and in Appendix A is similar to that used by Kraichnan [21] for turbulent velocity fields, and by Maradudin *et al.* [20] for the study of backscattering of light from random surfaces. Other authors use another strategy where the amplitudes of the velocity vector corresponding to different wave vectors are deterministically prescribed [22]. We have tested a similar approach where the random field is generated from the pure spatial correlation function $C_x(r)$

$$T'(x,t) = \theta\left[\frac{\alpha(t)}{\sqrt{L_x}}\widehat{C}_x^{1/2}(0) + \sum_{k=1}^{M}\frac{2}{\sqrt{L_x}}\widehat{C}_x^{1/2}\left(\frac{2\pi k}{L_x}\right)\cos\left(\frac{2\pi k x}{L_x}+\varphi_k(t)\right)\right], \quad (4)$$

where $\varphi_k(t)$ is a uniform random phase in the range $0 \leqslant \varphi_k(t) \leqslant 2\pi$, and $\alpha(t)$ is a uniform random number in the range $-\sqrt{3} \leqslant \alpha(t) \leqslant +\sqrt{3}$, in order to satisfy $\overline{T'(x,t)T'(x,t)}^t = \theta^2$. This approach is less rigorous than the previous one (equation (3)), and does not account for temporal correlations. However, the deterministic choice of the amplitudes in equation (4) leads to a faster convergence of the stochastic simulation. Band-integrated intensities (see Section 4) computed from both procedures differ by only 5% in the worst cases of optically thick medium or for Λ/L_x as high as 1, with $\theta/T_0 = 0.4$. Nevertheless, in the following we use the more general approach (equation (3)) in order to include both spatial and temporal correlations.

Correlation functions

The space–time correlation function $C(r,\tau)$ is assumed to be the product of the two-point/one-time correlation function $C_x(r)$ and the one-point/two-time correlation function $C_t(\tau)$

$$C(r,\tau) = C_x(r)C_t(\tau). \quad (5)$$

This assumption is used by other authors (cf. for example ref. [11]), even if there is no theoretical support for it. In order to investigate the influence of this approximation, calculations were also undertaken following Taylor's hypothesis. Two cases corresponding to a mean flow perpendicular and parallel to the observation direction have been considered. The function $C(r,\tau)$ cannot be split in the form $C_x(r)C_t(\tau)$ in these cases. The results show that the time-averaged emitted intensity computed from Taylor's hypothesis (both perpendicular and parallel cases) do not differ significantly from that obtained by using equation (5) (less than 1% in the perpendicular case and less than 2% in the parallel case, for a single absorption line). Equation (5) is then used in the following analysis. The analytical form adopted for $C_t(\tau)$ is

$$C_t(\tau) = \exp\left(-\frac{\tau}{t_c}\right), \quad (6)$$

where t_c is the integral time-scale. The particular form of $C_t(\tau)$ and the choice of t_c may have an important influence on the temporal spectrum of the emitted intensities, but not on the moments of these intensities. On the other hand, the total lapse of time t_0 considered in equation (3) must contain several integral time-scales in order to allow an acceptable convergence of the stochastic simulation. We use here $t_0 \simeq 500t_c$.

The spatial correlation function for temperature or concentration fluctuations generally exhibits an exponential decrease for intermediate values of the distance of separation, but it may become negative for higher values of r [23, 24]. The only rigorous limitation for the choice of $C_x(r)$ is that it must have a real and positive Fourier transform and satisfy $-C_x(0) \leqslant C_x(r) \leqslant C_x(0)$. In this study we use three analytical forms for $C_x(r)$

$$C_x(r) = e^{-r/\Lambda}, \quad 0 \leqslant r \leqslant L_x \quad (7a)$$

$$C_x(r) = \frac{\sin(\pi r/2\Lambda)}{(\pi r/2\Lambda)}, \quad 0 \leqslant r \leqslant L_x \quad (7b)$$

$$C_x(r) = 1 - \frac{r}{2\Lambda}, \quad 0 \leqslant r \leqslant 2\Lambda \quad (7c)$$

$$= 0, \quad 2\Lambda \leqslant r \leqslant L_x$$

where Λ is the integral length-scale satisfying

$$\int_0^{+\infty} C_x(r)\,dr = \Lambda.$$

Contrary to t_c, Λ is a variable parameter of this study. The results obtained by using the above analytical form of $C_x(r)$ are compared and discussed in Sections 3 and 4. Figure 1 shows typical correlation functions computed from the stochastic scalar fields as described above (with the ergodic hypothesis), averaged over 10 000 time realizations. The convergence to the theoretical functions is not wholly satisfactory; however, the convergence of the radiative intensities is much better.

3. ISOLATED LORENTZ LINE

Before studying the effects of turbulence on real gas radiation in a wide spectral range, we first consider the case of an isolated line in order to point out the main parameters of the problem and to gain insight

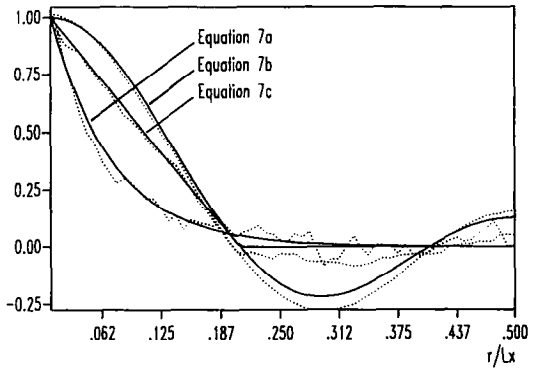

FIG. 1. The three theoretical correlation functions used in this study (solid lines). The dashed lines are the correlation functions averged over 10000 time realizations for an arbitrary position. $\Lambda/L_x = 0.1$.

concerning the interpretation of the results given in the following sections. The results of this section are also useful for optical diagnostics using the properties of isolated lines in turbulent media. Only temperature fluctuations are considered in this section and also in the following one.

If we assume that the real part of the refractive index of the medium is equal to 1, the instantaneous spectral intensity I_ν from the turbulent medium in the Ox direction is given by

$$I_\nu = \int_0^{L_x} \kappa_\nu(x) I_\nu^b(x) \exp\left(-\int_x^{L_x} \kappa_\nu(x')\,dx'\right) dx, \quad (8)$$

where the local absorption coefficient κ_ν and blackbody function I_ν^b vary with time and position since both depend on temperature. κ_ν is given for an isolated Lorentz line centered at the wave number ν_0, by

$$\kappa_\nu = x_a p S(T) \frac{1}{\pi} \frac{\gamma(T)}{\gamma^2(T) + (\nu - \nu_0)^2}, \quad (9)$$

where x_a is the molar fraction of the absorbing species, p the total pressure (in atmospheres), $S(T)$ the line strength and $\gamma(T)$ the half-width at half-maximum. In local thermodynamic equilibrium, the line strength temperature dependence is given by [25]

$$S(T) = S(T_s) \frac{T_s}{T} \frac{Q(T_s)}{Q(T)} \exp\left[-\frac{E''}{k}\left(\frac{1}{T} - \frac{1}{T_s}\right)\right] \times \frac{1 - \exp(-hc\nu_0/kT)}{1 - \exp(-hc\nu_0/kT_s)}. \quad (10)$$

In this equation, $Q(T)$ designates the rovibrational partition function of the considered absorbing molecule, E'' is the energy of the lower level of the transition, and k, h, and c are the Boltzmann constant, the Planck constant and speed of light, respectively. T_s is a reference temperature.

A Taylor expansion of the spectrally integrated radiative intensity

$$I = \int_{-\infty}^{+\infty} I_\nu \, d\nu$$

shows that, at least under some conditions, deviations from the isothermal medium intensity are mainly due to the derivatives $\partial^2 I_\nu^b/\partial T^2$, $\partial^2 S/\partial T^2$ and $(\partial I_\nu^b/\partial T)(\partial S/\partial T)$ (see Appendix B). It follows from equation (10) that line intensity variations with temperature are very sensitive to the value of E'' which is then an important parameter in this study. This fact was noticed by Pearce and Varma who considered only relatively high values of E'' in their study [15].

Numerical simulations have been carried out for a CO absorption line centered near $\nu_0 = 2124$ cm^{-1} with the average temperature $T_0 = 1000$ K. The CO partition function was computed from the polynomial fit of Gamache *et al.* [26] and $\gamma(T)$ was taken as [27]

$$\gamma(T) = 0.084 p \left(\frac{296}{T}\right)^{0.69} \text{cm}^{-1}. \quad (11)$$

The varying parameters in these numerical simulations are: the ratio Λ/L_x in the range $1/30 \leqslant \Lambda/L_x \leqslant 1$, E'' from 100 to 4000 cm^{-1}, the ratio θ/T_0 from 0. to 0.4, and the optical thickness at line center $u = (x_a p S(T_0) L_x)/(\pi\gamma(T_0))$ from 10^{-2} to 10. The spectral integration of radiative intensity is carried out by using a 16 point Gauss quadrature for a spectral range containing more than 95% of the intensity of the line.

Figure 2 shows some spectral results for $\theta/T_0 = 0.4$ with two values of E'' computed from the three differ-

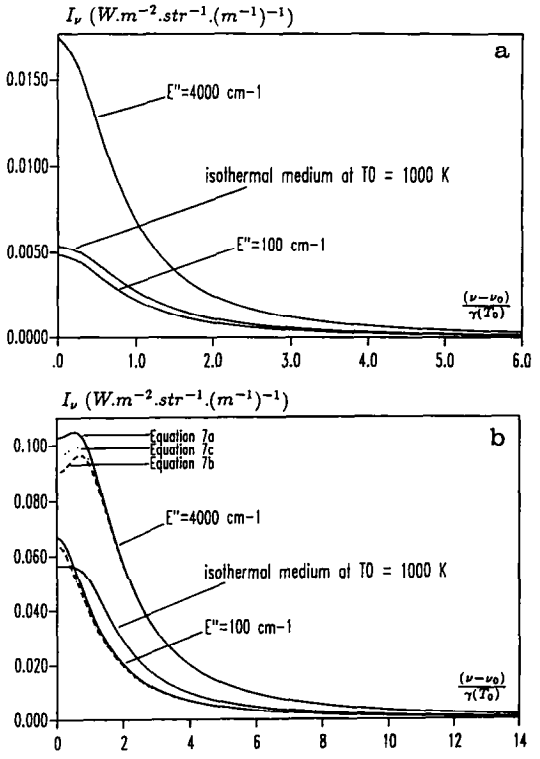

FIG. 2. Spectral radiative intensity from temperature fluctuating and isothermal media for two E'' values and three spatial correlation functions. $\theta/T_0 = 0.4$, $\Lambda/L_x = 0.2$, $T_0 = 1000$ K. The optical thickness at line center is $u = 0.1$ (a) and $u = 10$ (b).

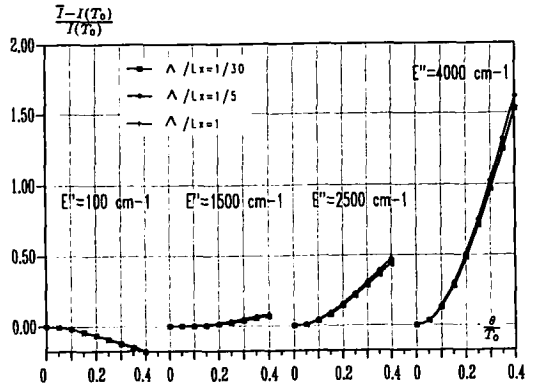

FIG. 3. Relative differences between nonisothermal and isothermal radiative intensities integrated over an isolated Lorentz line centered at $\nu_0 = 2124\ \text{cm}^{-1}$ for different E'' and Λ/L_x values. $u = 0.01$, $T_0 = 1000$ K, $p = 1$ atm, $L_x = 0.2$ m.

ent spatial correlation functions given by equations (7a–c). For an optically thin medium the monochromatic intensities are not sensitive to the shape of the correlation function (Fig. 2a). To the contrary, for an optically thick medium (Fig. 2b) and high values of E'', differences up to 13% are observed at line center, for which only a small fraction of the column contributes to the emission. However, when the intensities are integrated over the entire line, the differences remain limited to 4%. Figure 2 shows that the line shape may be strongly modified by temperature fluctuations, as noticed by Pearce and Varma [15]. In addition, it appears that total turbulence contributions are negative for $E'' = 100\ \text{cm}^{-1}$ since the terms containing $(\partial S/\partial T)$ are negative and dominate in this case. Turbulence contributions are positive in the case $E'' = 4000\ \text{cm}^{-1}$ and reach nearly 200% at line center. Relative differences between the spectrally integrated intensities, corresponding to turbulent and isothermal media, are shown in Figs. 3 and 4 for two optical thicknesses $u = 10^{-2}$ and $u = 10$, respectively. Turbulence contributions increase strongly with the turbulence intensity θ/T_0, but the sign of this contribution depends on the energy E'' of the lower level as seen above. Simple analytical calculations of

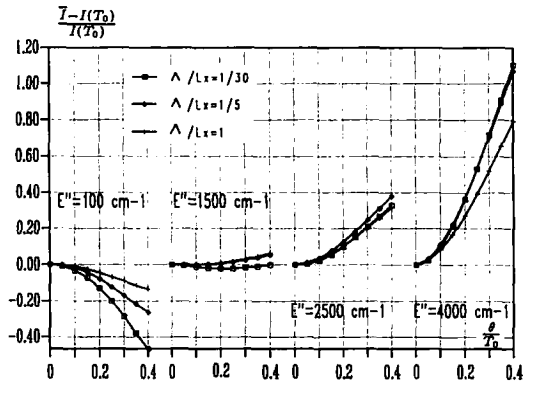

FIG. 4. Same as in Fig. 3 except $u = 10$.

$$S(T_0)\frac{\partial^2 I^b_{\nu_0}}{\partial T^2} + I^b_{\nu_0}(T_0)\frac{\partial^2 S}{\partial T^2} + 2\frac{\partial I^b_{\nu_0}}{\partial T}\frac{\partial S}{\partial T}$$

show that this sum is negative for $E'' < 1390\ \text{cm}^{-1}$ and positive beyond this value in the conditions $T_0 = 1000$ K and $\nu_0 = 2124\ \text{cm}^{-1}$. The results shown in Figs. 3 and 4 are in qualitatively good agreement with Taylor expansions given in Appendix B. However, this E'' limit value depends on the centerline position ν_0 and decreases when ν_0 tends to the value which maximizes $\partial^2 I^b_{\nu_0}/\partial T^2(T_0)$. From these considerations, turbulence effects are expected to be higher in the spectral regions where most of the absorption lines start from high rovibrational levels, as is often the case in band wings. The effects of turbulence structure (Λ/L_x) are more noticeable in the case of optically thick media, but these effects remain small in comparison with those of E'' and θ/T_0. Finally, it is worth noting that the relative differences decrease slightly when the optical thickness increases.

4. NARROW-BAND MODEL CALCULATIONS

Radiative properties of CO_2 and H_2O, averaged over spectral ranges of width $\Delta\nu = 25\ \text{cm}^{-1}$, are modelled here using a statistical narrow-band model. Absorption lines are assumed to be randomly located inside $\Delta\nu$ and their intensities obey an exponential-tailed-inverse distribution law [28]. It was shown that this model leads to the best agreement with line by line calculations for CO_2 and H_2O [29]. The temperature dependent parameters of this model are deduced from high temperature line by line calculations [30, 31]. If we assume that the blackbody intensity remains constant inside $\Delta\nu$, the instantaneous radiative intensity $I_{\Delta\nu}$, averaged over $\Delta\nu$, is given by

$$I_{\Delta\nu} = \int_0^{L_x} I^b_\nu(x)\frac{\partial \tau_{\Delta\nu}}{\partial x}(x, L_x)\,\mathrm{d}x, \qquad (12)$$

where $\tau_{\Delta\nu}(x, L_x)$ is the transmissivity of the nonisothermal column (x, L_x) averaged over $\Delta\nu$. This transmissivity is computed by using the Curtis–Godson approximation which has been studied elsewhere [32, 29]. We have investigated four CO_2 absorption bands and four H_2O bands for which the minimum and maximum wave numbers are given in Table 1. In

Table 1. Wave number limits of four CO_2 and four H_2O bands considered in this study

Band number	Gas	min (cm^{-1})	min (μm)	max (cm^{-1})	max (μm)
1	CO_2	475	21.052	1050	9.534
2	CO_2	2050	4.878	2425	4.124
3	CO_2	3400	2.941	3800	2.631
4	CO_2	4800	2.083	5175	1.932
5	H_2O	150	66.666	1075	9.302
6	H_2O	1100	9.091	2300	4.348
7	H_2O	2900	3.448	4200	2.381
8	H_2O	4900	2.041	5700	1.754

all computations, we consider H_2O–N_2 or CO_2–N_2 mixtures with the following conditions: $T_0 = 1000$ K, $x_{H_2O} = 0.1$ or $x_{CO_2} = 0.1$, $p = 1$ atm, and $L_x = 1$ m. The other parameters are Λ/L_x, which is varied in the range (1/30, 1), and θ/T_0 in the range (0, 0.4). On the other hand, we distinguish between the case of radiation directly from the hot turbulent medium, and the case of radiation emitted by this hot medium and partially transmitted through a cold homogeneous and isothermal medium. The first case is considered in order to simulate some typical heat transfer applications (e.g. furnaces or combustion chambers for propulsion), while the second case is related to teledetection applications or accidental fire radiation transmitted through air. The cold column is 100 m long at 300 K and the absorbing gas molar fractions are x_{CO_2} or $x_{H_2O} = 0.02$.

Figures 5 and 6 show low-resolution spectral intensities for the 4.3 μm CO_2 band and the 2.7 μm H_2O band, respectively, with the cold column (Figs. 5(b) and 6(b)) and without the cold column (Figs. 5(a) and 6(a)). Results corresponding to temperature fluctuating hot media with $\theta/T_0 = 0.35$ and $\Lambda/L_x = 0.2$ are compared in these figures to those corresponding to isothermal media. In addition, results from the three analytical forms of the correlation function are

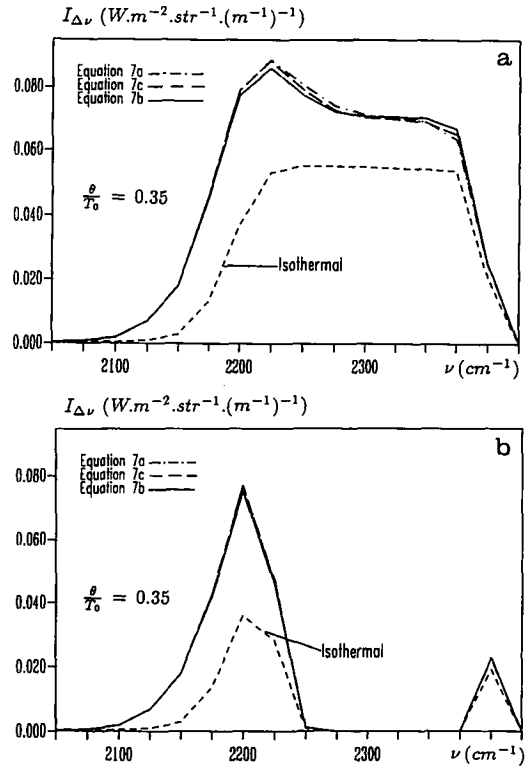

FIG. 5. Radiative intensity averaged over 25 cm^{-1} in the 4.3 μm CO_2 band, computed from three spatial correlation functions: (a) hot medium alone with $L_x = 1$ m, $x_{CO_2} = 0.1$, $p = 1$ atm, $T_0 = 1000$ K, $\Lambda/L_x = 0.2$; (b) the same hot medium is viewed through a cold isothermal medium with $L = 100$ m, $x_{CO_2} = 0.02$, $p = 1$ atm, and $T = 300$ K.

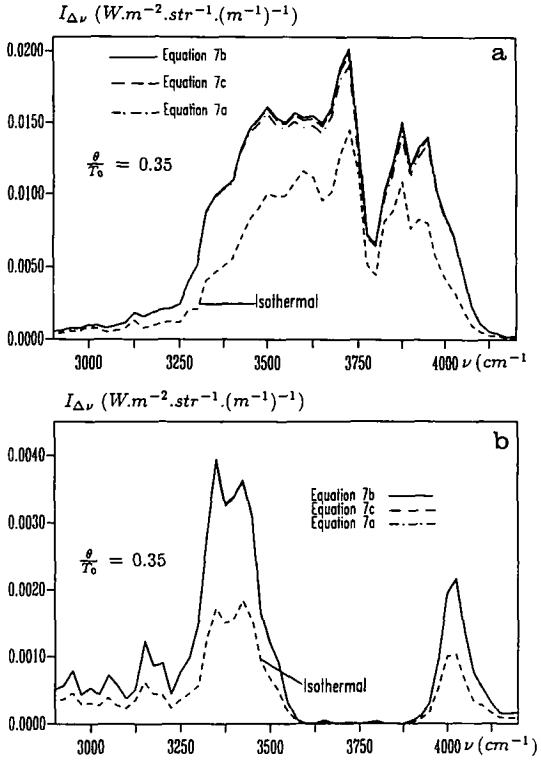

FIG. 6. Radiative intensity averaged over 25 cm^{-1} in the 2.7 μm H_2O band, computed from three spatial correlation functions: (a) hot medium alone with $L_x = 1$ m, $x_{H_2O} = 0.1$, $p = 1$ atm, $T_0 = 1000$ K, $\Lambda/L_x = 0.2$; (b) the same hot medium is viewed through a cold isothermal medium with $L = 100$ m, $x_{H_2O} = 0.02$, $p = 1$ atm, and $T = 300$ K.

compared. Radiative intensities are increased by a factor up to three in some spectral regions when temperature fluctuations are accounted for. In teledetection situations, radiation at band centers is totally absorbed by the cold medium and the only significant intensity remaining occurs in band wings. These regions generally contain many absorption lines starting from high energy levels (hot lines) with small intensities at low temperature. Turbulence effects are expected to be the most important for these lines, as discussed in the previous section. On the other hand, differences up to 5% are found when different correlation functions are used in the low-resolution computation. As for the study of an isolated line, the greater differences are obtained in the optically thick parts of the spectrum. The results in the teledetection situation are nearly insensitive to the shape of $C_x(r)$. In all cases, the integrated intensity over the band is affected by less than 3.5% when the shape of $C_x(r)$ is changed. All the following calculations are carried out by using the exponential shape of $C_x(r)$ (equation (7a)).

Relative differences between radiative intensities integrated over the whole band computed with and without turbulence effects are shown on Fig. 7 for CO_2 bands, and Fig. 8 for H_2O bands. Results corresponding to different Λ/L_x values are illustrated in

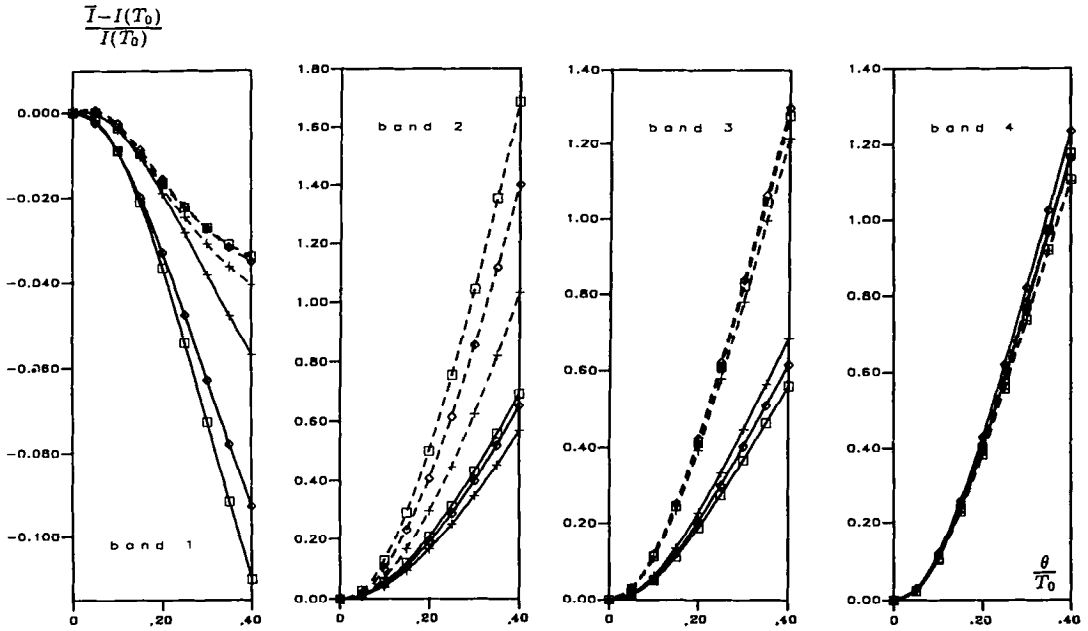

FIG. 7. Relative differences between nonisothermal and isothermal band integrated radiative intensities for CO_2 bands. —— hot turbulent medium alone with $L_x = 1$ m, $x_{CO_2} = 0.1$, $p = 1$ atm, $T_0 = 1000$ K. ---- the same hot medium viewed through a cold isothermal medium with $L = 100$ m, $x_{CO_2} = 0.02$, $p = 1$ atm, and $T = 300$ K. Wave number limits for these bands are given in Table 1. + $\Lambda/L_x = 1$, ◇ $\Lambda/L_x = 0.2$, □ $\Lambda/L_x = 0.033$.

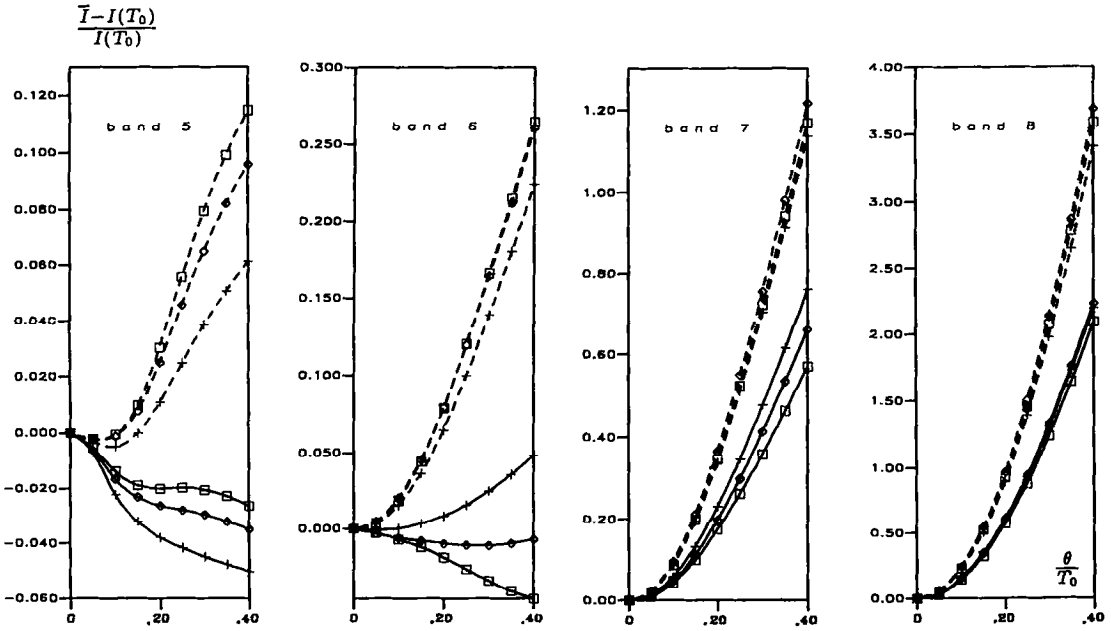

FIG. 8. Relative differences between nonisothermal and isothermal band integrated radiative intensities for H_2O bands. —— hot turbulent medium alone with $L_x = 1$ m, $x_{H_2O} = 0.1$, $p = 1$ atm, $T_0 = 1000$ K. ---- the same hot medium viewed through a cold isothermal medium with $L = 100$ m, $x_{H_2O} = 0.02$, $p = 1$ atm, and $T = 300$ K. Wave number limits for these bands are given in Table 1. + $\Lambda/L_x = 1$, ◇ $\Lambda/L_x = 0.2$, □ $\Lambda/L_x = 0.033$.

these figures. Turbulence contributions increase generally with θ/T_0, but under some conditions, temperature fluctuations may lead to a small decrease in the radiative intensities (e.g. the first CO_2 band). This may be easily explained by the spectral location of the band for a given temperature. In fact, the maximum of $\partial I_\nu^b/\partial T$ occurs near $\nu/T = 2.66\ \text{cm}^{-1}\ \text{K}^{-1}$, and $\partial^2 I_\nu^b/\partial T^2$ is maximum for $\nu/T = 3.79\ \text{cm}^{-1}\ \text{K}^{-1}$. For the CO_2 band centered near 650 cm^{-1}, variations of blackbody intensity with temperature are quasi-linear and the nonlinearities of line intensity variations play the predominant role in turbulence effects. However, except for the 'far-infrared' bands, turbulence leads to an increase in the integrated radiative intensities, reaching about 220% in the case of a hot medium alone and 370% in the case of a hot medium viewed through a cold one, for a turbulence intensity $\theta/T_0 = 0.4$. The increase in radiative intensities in the case of teledetection situations is practically two times greater than that observed for the hot medium alone for the bands 2, 3, 7 and 8. But this conclusion cannot be generalized in all conditions since this depends on the spectroscopic parameters of the lines constituting the considered band.

On the other hand, it is seen from Figs. 7 and 8 that the integral length-scale of turbulence has an influence in the spectral regions where the medium tends to be optically thick (e.g. the CO_2 band at 4.3 μm), otherwise, temporal and spatial variations act in a similar manner, as discussed for an isolated Lorentz line. Figure 9 shows the effects of turbulence on the emitted intensities, integrated over all the spectrum in the case of a hot column alone, and containing CO_2 or H_2O. Relative differences with the isothermal medium intensities are plotted for different values of the mean temperature and molar fraction, for the conditions $\Lambda/L_x = 0.2$ and $\theta/T_0 = 0.4$. It is shown that turbulence contributions decrease quickly when the mean temperature increases from 800 to 2000 K. This is due mainly to the fast decrease of the integrated second derivative

$$\frac{\int_0^{+\infty} \frac{\partial^2 I_\nu^b}{\partial T^2} \mathrm{d}\nu}{\int_0^{+\infty} I_\nu^b \,\mathrm{d}\nu}$$

with temperature. For a given turbulence intensity, temperature fluctuation effects are smaller for high temperature flames. In addition, integrated turbulence effects decrease when the optical thickness decreases. This may be understood in terms of the combined effects of radiative properties and blackbody variations with temperature. In fact, the cross second order derivatives, which have a negative contribution to the averaged intensity, decrease when the optical thickness increases.

The stochastic simulation used in this study also enables a statistical description of the fluctuations of the radiative intensity around its mean value. Nevertheless, the power spectral density of these fluctuations depend mostly on the temporal correlation function used, while the different moments of these fluctuations do not. Figure 10 shows the standard deviation of the fluctuations of the spectrally integrated intensity around its mean value for CO_2–N_2 mixtures as a function of the mean temperature and molar fraction. This standard deviation increases with the optical thickness, since only a small part of the

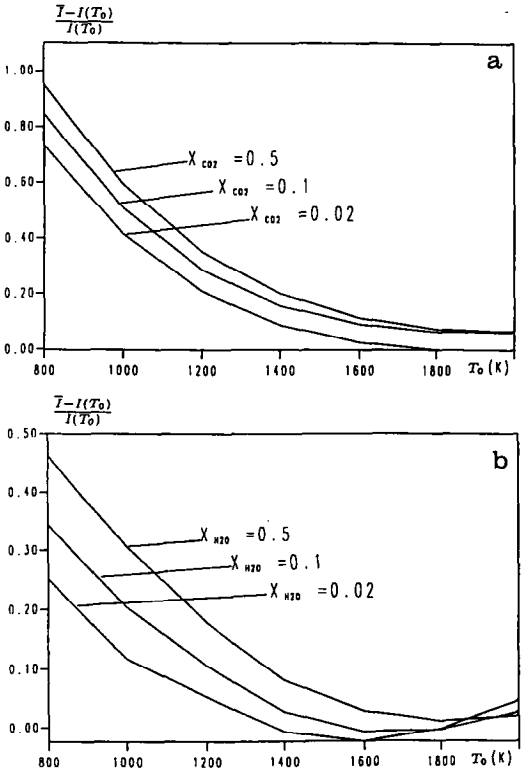

FIG. 9. Relative differences between nonisothermal and isothermal infrared integrated radiative intensities, as function of the mean temperature and molar fraction $L_x = 1$ m, $p = 1$ atm, $\theta/T_0 = 0.4$, $\Lambda/L_x = 0.2$. CO_2–N_2 mixtures (a) and H_2O–N_2 mixtures (b).

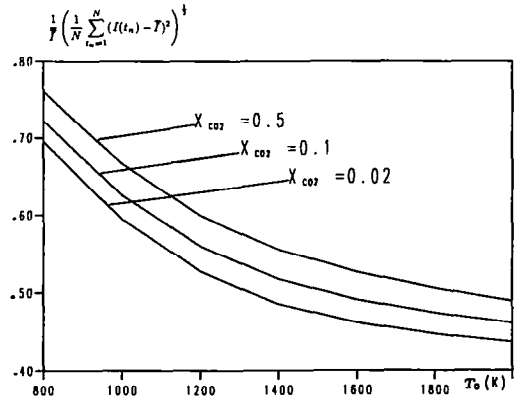

FIG. 10. Standard deviation of the fluctuation of the infrared integrated radiative intensity for CO_2–N_2 mixtures as function of the mean temperature and CO_2 molar fraction. $L_x = 1$ m, $p = 1$ atm, $\theta/T_0 = 0.4$, $\Lambda/L_x = 0.2$.

column (with a large fluctuation of its mean temperature), contributes to the emitted radiation in the case of an optically thick medium. For an optically thin medium the standard deviation depends mostly on the number of large eddies contained in the column and increases with the ratio Λ/L_x. It is also worth noting that, in the conditions of Fig. 10, the standard deviation remains as high as 50% when the mean temperature increases up to 2000 K, although the turbulence contribution to the mean intensity becomes very small.

5. MOLAR FRACTION FLUCTUATIONS

We will first consider the case of molar fraction fluctuations in an isothermal medium and then the general case of combined molar fraction and temperature fluctuations.

For an isothermal medium, the nonlinearity in the relation between the absorption coefficient and the emitting gas molar fraction is only due to the variations of Lorentz line-widths with different collision partners. These variations generally lead to very small changes in the emitted radiation since line intensities are unmodified. On the other hand, radiative intensity from an isothermal and homogeneous medium may be written, with the narrow-band model used here, as

$$I_{\Delta\nu} = \Delta\nu I^b_{\nu_0}\left\{1-\exp\left[-\frac{2\bar{\gamma}}{\bar{\delta}}\times\left(\left(1+\frac{x_a p L_x \bar{k}\bar{\delta}}{\bar{\gamma}}\right)^{1/2}-1\right)\right]\right\}, \quad (13)$$

where $\bar{k}$, $\bar{\gamma}$ and $\bar{\delta}$ are the model parameters [32]. The nonlinearities due to the exponential term remain limited to a few percent when considering the emitted radiation from an isothermal medium with fluctuating x_a values. This is not the case for radiation transmitted by a concentration fluctuating medium.

These small effects of molar fraction fluctuations alone have been tested numerically for the CO_2 and H_2O bands given in Table 1. Relative variations in band-integrated radiative intensities are limited to about 3% for concentration fluctuation intensities as high as 0.35.

In the case of combined concentration and temperature fluctuations, Song and Viskanta [16] show that turbulence effects depend upon whether concentration and temperature variations are positively or negatively correlated. The signs and amplitudes of the cross-correlation depend on the application under consideration, but we may expect that in combustion applications the main contribution to emission is due to combustion products at elevated temperatures. Concentration and temperature should then be positively correlated. We investigate here both cases of positive and negative perfect cross-correlations. The spatial autocorrelation functions of molar fraction and temperature fluctuations are assumed to obey the same exponential decrease (equation (7a)) with the same integral scale Λ. The cross-correlation function is then given by

$$R_{x_a T}(r) = \frac{\langle x'_a(x,t)T'(x+r,t)\rangle}{\sigma\theta} = \pm\exp(-r/\Lambda), \quad (14)$$

where σ is the r.m.s. value of the molar fraction fluctuations, and the signs + and − correspond to positive and negative perfect cross-correlations, respectively. Computations are carried out in the same conditions as in the previous section (column length, mixtures, and mean temperature and molar fraction values), with σ/x_a varying in the range (0, 0.35).

Figure 11 shows the relative differences between band integrated radiative intensities computed with and without scalar fluctuations for the 4.3 μm CO_2 band and the 2.7 μm H_2O band. Both positive and negative correlation cases are illustrated in this figure. It is shown that positive correlations lead to a significant increase in the turbulence contribution to radiative intensities, while negative correlations tend to decrease its effect. In fact, in the positive correlation

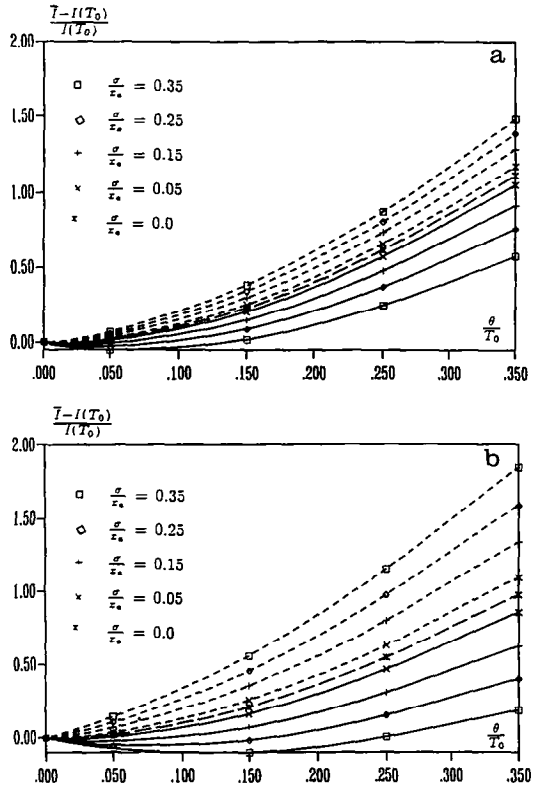

FIG. 11. Relative differences between band integrated radiative intensities for the 4.3 μm CO_2 band (a) and for the 2.7 μm H_2O band (b), computed with and without temperature and molar fraction fluctuations. The hot medium with L_x = 1 m, x_{CO_2} or $x_{H_2O} = 0.1$, $p = 1$ atm, $T_0 = 1000$ K, $\Lambda/L_x = 0.2$, is viewed through a cold isothermal medium with L = 100 m, x_{CO_2} or $x_{H_2O} = 0.02$, $p = 1$ atm, and $T = 300$ K. —— negative cross-correlations, ---- positive cross-correlations.

case the hot regions of the radiating medium contain more emitting gases and this tends to emphasize the nonlinearities of Planck's function and line intensity variations with temperature. Results similar to those shown in Fig. 11 are found for the eight CO_2 and H_2O absorption bands, with or without a cold absorbing medium, and for any value of Λ/L_x in the studied range.

Finally, some numerical simulations were carried out for noncorrelated temperature and concentration fluctuations. The results show that concentration fluctuations have a very small effect on radiative intensities in this case (less than 4%).

6. CONCLUSIONS

We have performed a theoretical study concerning the effects of temperature and concentration fluctuations on mean radiative intensities from a hot, turbulent, statistically homogeneous and stationary gas mixture. The fluctuating fields have been generated from space–time correlation functions and realistic representations of molecular gas absorption spectra have been used. We have shown that the contribution of turbulence to the mean radiative intensity is not very sensitive to the shape of the spatial correlation function. It does not depend on the integral length-scale of turbulence if the medium contains several optically thin eddies. For a given absorption band, the most influential parameters are the fluctuation intensities, band spectral location (with respect to a given value of the men temperature), spectroscopic parameters of the absorption lines constituting the band, and to a lesser extent the integral length-scale of turbulence and the medium opacity. Mean radiative intensities are generally increased when turbulent fluctuations are taken into account, but the turbulence contribution may be negative for some far-infrared bands. On the other hand, it is found that the effects of turbulence are greater when the hot emitting medium is seen through a cold absorbing one, since nonlinearities due to line intensities are generally stronger for the 'hot lines' located in the band wings. The contribution of turbulence to the intensity, integrated over all the infrared spectrum, decreases quickly when the mean temperature increases in the range $800 \leqslant T_0 \leqslant 2000$ K. Concentration fluctuations in an isothermal medium have small effects, however, when they are combined with temperature fluctuations, the changes in radiative intensity due to temperature fluctuations alone are significantly increased for positive cross-correlations and decreased for negative correlations.

REFERENCES

1. A. A. Townsend, The effects of radiative transfer on turbulent flow of a stratified fluid, *J. Fluid Mech.* **4,** 361–375 (1958).
2. M. Coantic and O. Simonin, Radiative effects on turbulent temperature spectra and budgets in the planetary boundary layer, *J. atmos. Sci.* **41,** 2629–2651 (1984).
3. A. Soufiani, Temperature turbulence spectrum for high temperature radiating gases, *J. Thermophysics* **5,** 489–494 (1991).
4. G. Cox, On radiant heat transfer from turbulent flames, *Comb. Sci. and Tech.* **17,** 75–78 (1977).
5. F. C. Lockwood and A. S. Naguib, The prediction of the fluctuations in the properties of free, round-jet, turbulent, diffusion flames, *Combust. Flame* **24,** 109–124 (1975).
6. S. M. Jeng, M. C. Lai and G. M. Faeth, Nonluminous radiation in turbulent buoyant axisymmetric flames, *Comb. Sci. and Tech.* **40,** 41–43 (1984).
7. G. M. Faeth, S. M. Jeng and J. P. Gore, Radiation from flames, In *Heat Transfer in Fire and Combustion Systems* (Edited by C. K. Law *et al.*), HTD **45,** pp. 137–151, ASME, New York (1985).
8. G. M. Faeth, Heat and mass transfer in flames, *Proc. 8th Int. Heat Transfer Conf.*, vol. I, pp. 151–160 (1986).
9. J. P. Gore, S. M. Jeng and G. M. Faeth, Spectral and total radiation properties of turbulent carbon monoxide/air diffusion flames, *AIAA J.* **25,** 339–345 (1987).
10. J. P. Gore, S. M. Jeng and G. M. Faeth, Spectral and total radiation properties of turbulent hydrogen/air diffusion flames, *J. Heat Transfer* **109,** 165–171 (1987).
11. M. E. Kounalakis, J. P. Gore and G. M. Faeth, Mean and fluctuating radiation properties of nonpremixed turbulent carbon monoxide/air flames, *J. Heat Transfer* **111,** 1021–1030 (1989).
12. M. E. Kounalakis, Y. R. Sivathanu and G. M. Faeth, Infrared radiation statistics of nonluminous turbulent diffusion flames, *J. Heat Transfer* **113,** 437–445 (1991).
13. Y. R. Sivathanu, M. E. Kounalakis and G. M. Faeth, Soot and continuum radiation statistics of luminous turbulent diffusion flames, *Twenty Third Symposium (International) on Combustion*, Pittsburgh, PA, pp. 1543–1550 (1990).
14. Y. R. Sivathanu, J. P. Gore and J. Dolinar, Transient scalar properties of strongly radiating jet flames, *Comb. Sci. and Tech.* **76,** 45–66 (1991).
15. B. E. Pearce and A. K. Varma, Radiation-turbulence interaction in a tactical missile exhaust plume, *AIAA 16th Thermophysics Conference*, June 23–25, Palo Alto, pp. 1110–1121 (1981).
16. T. H. Song and R. Viskanta, Interaction of radiation with turbulence: application to a combustion system, *J. Thermophysics* **1,** 56–62 (1987).
17. A. Soufiani, P. Mignon and J. Taine, Radiation effects on turbulent heat transfer in channel flows of infrared active gases. In *Radiation Heat Transfer: Fundamentals and Applications* (Edited by Smith *et al.*), HTD **137,** pp. 141–148, ASME, New York (1990).
18. J. W. Daily, Effect of turbulence on line-reversal temperature measurements, *J. Quant. Spectrosc. Radiat. Transfer* **17,** 339–341 (1977).
19. M. Charpenel, Mesures instantanées par pyrométrie infrarouge de temperature de gaz de combustion. Application a la turbulence thermique, *Rev. Phys. Appl.* **14,** 491–508 (1979).
20. A. A. Maradudin, T. Michel, A. R. McGurn and E. R. Mendez, Enhanced backscattering of light from a random grating, *Ann. Phys.* **203,** 255–307 (1990).
21. R. H. Kraichnan, Decay of isotropic turbulence in the direct-interaction approximation, *Phys. Fluids* **7,** 1030–1048 (1964).
22. M. Karweit, Ph. Blanc-Benon, D. Juve and G. Comte-Bellot, Simulation of the propagation of an acoustic wave through a turbulent velocity field: a study of phase variance, *J. Acoust. Soc. Am.* **89,** 52–62 (1991).
23. A. S. Monin and A. M. Yaglom, *Statistical Fluid Mechanics: Mechanics of Turbulence*, Vol. 2. The MIT Press, Cambridge (1981).

24. H. A. Becker, H. C. Hottel and G. C. Williams, The nozzle-fluid concentration field of the round, turbulent, free jet, *J. Fluid Mech.* **30,** 285–303 (1967).
25. S. S. Penner, *Quantitative Molecular Spectroscopy and Gas Emissivities.* Pergamon Press, London–Paris (1959).
26. R. R. Gamache, R. L. Hawkins and L. S. Rothman, Total internal partition sums in the temperature range 70–3000 K: atmospheric linear molecules, *J. mol. Spec.* **142,** 205–219 (1990).
27. A Soufiani and J. Taine, High-resolution spectroscopy temperature measurements in laminar channel flows, *Appl. Optics* **27,** 3754–3760 (1988).
28. W. Malkmus, Random Lorentz band model with exponential tailed S^{-1} line-intensity distribution, *J. Opt. Soc. Am.* **57,** 323–329 (1967).
29. A. Soufiani, J. M. Hartmann and J. Taine, Validity of band model calculations for CO_2 and H_2O applied to radiative properties and conductive–radiative transfer, *J. Quant. Spectrosc. Radiat. Transfer* **33,** 243–257 (1985).
30. J. Taine, A line by line calculation of low-resolution radiative properties of CO_2–CO-transparent non-isothermal gas mixtures up to 3000 K, *J. Quant. Spectrosc. Radiat. Transfer* **30,** 371–379 (1983).
31. J. M. Hartmann, R. Levi Di Leon and J. Taine, Line-by-line and narrow-band-statistical model calculations for H_2O, *J. Quant. Spectrosc. Radiat. Transfer* **32,** 119–127 (1984).
32. S. J. Young, Nonisothermal band model theory, *J. Quant. Spectrosc. Radiat. Transfer* **18,** 1–28 (1977).
33. J. W. Goodman, *Statistical Optics.* Wiley, New York (1985).
34. V. P. Kabashnikov and G. I. Kmit, Influence of turbulent fluctuations on thermal radiation, *J. Appl. Spectroscopy* **31,** 963–967 (1979).

APPENDIX A: GENERATION OF THE STOCHASTIC SCALAR FIELDS

The formulation given in this appendix is an extension of the work of Maradudin *et al.* [20] for the case of space and time varying stochastic processes. The scalar field $T'(x, t)$ is a Gaussian, statistically homogeneous and stationary random field, and is described by the space–time autocorrelation function $C(r, \tau)$ (equation (2) in the full text). For the discrete point ($x_k = k\Delta x$, $t_l = l\Delta t$), $T'(x_k, t_l)$ is first written in the form

$$T'(x_k, t_l) = \theta \sum_{i=-\infty}^{+\infty} \sum_{j=-\infty}^{+\infty} W_{i,j} X_{i+k,j+l}, \tag{A.1}$$

where $X_{i,j}$ are Gaussian, independent, random variables with zero mean and a standard deviation of unity. The weights $W_{i,j}$ are to be prescribed deterministically from the statistical properties of $T'(x, t)$. From equation (2) and the properties of $X_{i,j}$, we have for any pair (m, n)

$$C(m\Delta x, n\Delta t) = \sum_{i=-\infty}^{+\infty} \sum_{j=-\infty}^{+\infty} W_{i,j} W_{i-m,j-n}. \tag{A.2}$$

The right-hand side of this equation can be approximated by the continuous integral

$$\sum_{i=-\infty}^{+\infty} \sum_{j=-\infty}^{+\infty} W_{i,j} W_{i-m,j-n} = \frac{1}{\Delta x \Delta t} \times \int_{-\infty}^{+\infty} \int_{-\infty}^{+\infty} W(x, t) W(x - m\Delta x, t - n\Delta t)\, \mathrm{d}x\, \mathrm{d}t. \tag{A.3}$$

Following the Wiener–Khinchin theorem (see for example ref. [33]), the Fourier transform of the double integral on the r.h.s. of equation (A.3) is equal to the power spectral density $|\hat{W}(k, w)|^2$ of $W(x, t)$, where $\hat{W}(k, w)$ is the Fourier transform of $W(x, t)$:

$$\hat{W}(k, w) = \int_{-\infty}^{+\infty} \int_{-\infty}^{+\infty} W(x, t)\, \mathrm{e}^{-\mathrm{i}(kx + wt)}\, \mathrm{d}x\, \mathrm{d}t. \tag{A.4}$$

The Fourier transform of equation (A.2) leads then to the possible values of $\hat{W}(k, w)$

$$\hat{W}(k, w) = \Delta x^{1/2} \Delta t^{1/2} \hat{C}^{1/2}(k, w), \tag{A.5}$$

where $\hat{C}(k, w)$ is the Fourier transform of $C(r, \tau)$. The weights $W_{i,j}$ can then be obtained by the inverse Fourier transform:

$$W_{i,j} = \int_{-\infty}^{+\infty} \int_{-\infty}^{+\infty} \frac{\mathrm{d}k\, \mathrm{d}w}{4\pi^2} \Delta x^{1/2} \Delta t^{1/2} \hat{C}^{1/2}(k, w)\, \mathrm{e}^{\mathrm{i}(ki\Delta x + wj\Delta t)}. \tag{A.6}$$

The scalar field $T'(x_k, t_l)$ may be computed from equations (A.1, A.6), but it is advantageous to use a discrete Fourier transform in order to exploit the fast speed of FFT algorithms. If we assume that the function $C(r, \tau)$ is periodic with periods L_x and t_0 with $L_x = 2M\Delta x$, $t_0 = 2N\Delta t$, and define the discrete Fourier transform as

$$\hat{W}_{k,w} = \frac{1}{\sqrt{2M}} \frac{1}{\sqrt{2N}} \sum_{i=-M}^{M-1} \sum_{j=-N}^{N-1} W_{i,j}\, \mathrm{e}^{-2\mathrm{i}\pi(ki/\sqrt{2M} + wj/\sqrt{2N})}, \tag{A.7}$$

and the inverse Fourier transform

$$W_{i,j} = \frac{1}{\sqrt{2M}} \frac{1}{\sqrt{2N}} \sum_{k=-M}^{M-1} \sum_{w=-N}^{N-1} \hat{W}_{k,w}\, \mathrm{e}^{2\mathrm{i}\pi(ki/\sqrt{2M} + wj/\sqrt{2N})}, \tag{A.8}$$

the relation between the discrete and continuous Fourier transforms, for sufficiently high values of M and N is

$$\hat{W}_{k,w} = \frac{1}{\sqrt{\Delta x}\sqrt{L_x}} \frac{1}{\sqrt{\Delta t}\sqrt{t_0}} \hat{W}\left(\frac{2\pi k}{L_x}, \frac{2\pi w}{t_0}\right). \tag{A.9}$$

If we replace $W_{i,j}$ and $X_{i,j}$ by their decomposition (A.8) in equation (A.1) and use the relation

$$\frac{1}{2M} \sum_{j=-M}^{M-1} \mathrm{e}^{\mathrm{i}(k+k')j} = \delta(k + k'), \tag{A.10}$$

where δ denotes the delta function, we obtain after some manipulation

$$T'(x_m, t_n) = \theta \sum_{k=-M}^{M-1} \sum_{w=-N}^{N-1} \hat{W}_{-k,-w} \hat{X}_{k,w}\, \mathrm{e}^{2\mathrm{i}\pi(mk/2M + nw/2N)}, \tag{A.11}$$

with $\hat{W}_{-k,-w} = \hat{W}_{k,w}$ from equation (A.5). Equations (A.5) and (A.9) lead to

$$T'(x_m, t_n) = \theta \sum_{k=-M}^{M-1} \sum_{w=-N}^{N-1} \times \frac{1}{\sqrt{L_x}} \frac{1}{\sqrt{t_0}} \hat{C}^{1/2}\left(\frac{2\pi k}{L_x}, \frac{2\pi w}{t_0}\right) \hat{X}_{k,w}\, \mathrm{e}^{2\mathrm{i}\pi(mk/2M + nw/2N)}. \tag{A.12}$$

$\hat{X}_{k,w}$ may be decomposed into real and imaginary parts

$$\hat{X}_{k,w} = \tfrac{1}{2}(A_{k,w} + \mathrm{i}B_{k,w}), \tag{A.13}$$

with

$$A_{k,w} = \frac{1}{\sqrt{M}} \frac{1}{\sqrt{N}} \sum_{i=-M}^{M-1} \sum_{j=-N}^{N-1} \times X_{i,j} \cos\left[2\pi\left(\frac{ki}{2M} + \frac{wj}{2N}\right)\right] = A_{-k,-w}, \tag{A.14}$$

$$B_{k,w} = -\frac{1}{\sqrt{M}} \frac{1}{\sqrt{N}} \sum_{i=-M}^{M-1} \sum_{j=-N}^{N-1} \times X_{i,j} \sin\left[2\pi\left(\frac{ki}{2M} + \frac{wj}{2N}\right)\right] = -B_{-k,-w}. \tag{A.15}$$

As the Fourier transform of a Gaussian function is itself Gaussian, the sequences $A_{k,w}$ and $B_{k,w}$ are themselves Gaus-

sian, independent, random variables with zero mean and a standard deviation of unity. Equation (A.12) leads to finally

$$T'(x_m, t_n) = \theta \sum_{k=-M}^{M-1} \sum_{w=-N}^{N-1} \frac{1}{2} \frac{1}{\sqrt{L_x}} \frac{1}{\sqrt{t_0}} \times (A_{k,w} + iB_{k,w}) \hat{C}^{1/2}\left(\frac{2\pi k}{L_x}, \frac{2\pi w}{t_0}\right) e^{2i\pi(mk/2M + nw/2N)}. \quad (A.16)$$

APPENDIX B: TAYLOR EXPANSION IN SOME LIMITING CASES

We consider here radiative intensities, integrated over an isolated Lorentz line, in two asymptotic cases of the ratio Λ/L_x. The case $\Lambda/L_x \gg 1$ is not physically realistic since the meaning of Λ itself is not clear. However, we can assume that this case corresponds to an isothermal medium with a uniform temperature varying only in time. In the case $\Lambda/L_x \ll 1$, the column of length L_x contains many large eddies and the instantaneous radiative intensity is practically independent of time, as long as the optical thickness of a column of length Λ is not too large. In both cases, we consider a uniform concentration field and study temperature fluctuation effects on radiative intensities by using a second order Taylor expansion.

B1: $\Lambda/L_x \gg 1$

Radiative intensity resulting from an isolated line and an isothermal medium may be written

$$I(T) = \int_{-\infty}^{+\infty} \{1 - \exp(-\kappa_\nu L_x)\} I_\nu^b(T)\, d\nu = I_{\nu_0}^b(T) W(S(T)), \quad (B.1)$$

where the blackbody intensity I_ν^b is assumed to be constant over the narrow spectral range around ν_0, inside which κ_ν differs significantly from 0. The equivalent line width $W(S(T))$ is given by

$$W(S(T)) = \int_{-\infty}^{+\infty} \{1 - \exp(-\kappa_\nu L_x)\}\, d\nu. \quad (B.2)$$

The decomposition of T into its mean and fluctuating parts $T = T_0 + T'$, and the introduction of the probability density function $p(T')$ of T', lead to the time averaged intensity

$$\bar{I}' = \int_{-\infty}^{+\infty} p(T') W(S(T_0 + T')) I_{\nu_0}^b(T_0 + T')\, dT'. \quad (B.3)$$

If we neglect line-width variations with temperature in comparison with those of line intensity, a second order Taylor expansion of (B.3) yields

$$\frac{\bar{I}' - I(T_0)}{\theta^2} = \underbrace{\frac{\partial W}{\partial S}\frac{\partial S}{\partial T}\frac{\partial I_{\nu_0}^b}{\partial T}}_{(a)} + \underbrace{\frac{I_{\nu_0}^b}{2}\left\{\frac{\partial W}{\partial S}\frac{\partial^2 S}{\partial T^2}\right.}_{(b)} + \underbrace{\left.\frac{\partial^2 W}{\partial S^2}\left(\frac{\partial S}{\partial T}\right)^2\right\}}_{(c)} + \underbrace{\frac{W(S(T_0))}{2}\frac{\partial^2 I_{\nu_0}^b}{\partial T^2}}_{(d)}, \quad (B.4)$$

where θ is the r.m.s. value of T'

$$\theta^2 = \int_{-\infty}^{+\infty} p(T') T'^2\, dT', \quad (B.5)$$

and the right-hand side of equation (B.4) is taken at $T = T_0$. Terms (a) and (b) in (B.4) may be positive or negative depending on the signs of $\partial S/\partial T$ and $\partial^2 S/\partial T^2$. (c) is a negative term for a Lorentzian line and (d) is positive.

B2: $\Lambda/L_x \ll 1$

The instantaneous radiative intensity at the point 0 is given by

$$I = \int_0^{L_x} I_{\nu_0}^b(x) \frac{\partial W(x)}{\partial x}\, dx, \quad (B.6)$$

with the equivalent line-width

$$W(x) = \int_{-\infty}^{+\infty} \left\{1 - \exp\left(-\int_0^{L_x} \kappa_\nu(x')\, dx'\right)\right\} d\nu. \quad (B.7)$$

If we use the Curtis–Godson approximation, the derivative $\partial W(x)/\partial x$ may be written [32]

$$\frac{\partial W(x)}{\partial x} = x_a S(x)\, y(x_e(x), \rho(x)), \quad (B.8)$$

with

$$x_e(x) = \frac{u(x) S_e(x)}{2\pi\gamma_e(x)}, \quad u(x) = x_a p x,$$

$$S_e(x) = \frac{1}{u(x)} \int_0^x x_a p S(x')\, dx',$$

$$\gamma_e(x) = \frac{1}{u(x) S_e(x)} \int_0^x x_a p S(x') \gamma(x')\, dx',$$

$$\rho(x) = \frac{\gamma(x)}{\gamma_e(x)},$$

and

$$y(x_e, \rho) = (2 - \rho)\frac{dF}{dx_e}(x_e) + (\rho - 1) F(x_e),$$

where $F(x_e)$ is the Ladenburg–Reiche function [32].

If we again neglect line width variations with temperature in comparison with those of line intensity ($\rho(x) = 1$), equation (B.6) reduces to

$$I = \int_0^{L_x} x_a p S(x) \frac{dF}{dx_e}(x_e(x)) I_{\nu_0}^b(x)\, dx. \quad (B.9)$$

A second order Taylor expansion of $x_e(x)$ leads to

$$x_e(x) = \frac{x_a p}{2\pi\gamma} \int_0^x S(x')\, dx' = x_0(x) + \alpha(x) + \beta(x), \quad (B.10)$$

with

$$x_0(x) = \frac{x_a p}{2\pi\gamma} x S(T_0), \quad \alpha(x) = \frac{x_a p}{2\pi\gamma} \int_0^x T'(x') \frac{dS}{dT} dx',$$

$$\beta(x) = \frac{x_a p}{2\pi\gamma} \int_0^x \frac{T'^2(x')}{2} \frac{d^2 S}{dT^2} dx'.$$

Replacement in equation (B.9) and then expanding $S(x)$ and $I_{\nu_0}^b(x)$ gives

$$I - I(T_0) = x_a p \int_0^{L_x} \left\{\left[S(T_0)\frac{\partial I_{\nu_0}^b}{\partial T} + I_{\nu_0}^b(T_0)\frac{\partial S}{\partial T}\right] T'(x) + \left[2\frac{\partial S}{\partial T}\frac{\partial I_{\nu_0}^b}{\partial T} + S(T_0)\frac{\partial^2 I_{\nu_0}^b}{\partial T^2} + I_{\nu_0}^b(T_0)\frac{\partial^2 S}{\partial T^2}\right]\frac{T'^2(x)}{2}\right\} \times \left\{\frac{dF}{dx_e}(x_0) + [\alpha(x) + \beta(x)]\frac{d^2 F}{dx_e^2}(x_0) + \ldots\right\} dx. \quad (B.11)$$

At this point, we may consider two limiting cases:

(i) In the weak absorption limit, $W(x)$ is proportional to $S(x)$ and $dF/dx_e(x_e(x))$ is equal to 1. The difference $I - I(T_0)$ is then proportional to

$$\frac{\theta^2}{2}\left[2\frac{\partial S}{\partial T}\frac{\partial I_{\nu_0}^b}{\partial T} + I_{\nu_0}^b(T_0)\frac{\partial^2 S}{\partial T^2} + S(T_0)\frac{\partial^2 I_{\nu_0}^b}{\partial T^2}\right], \quad (B.12)$$

where θ is the spatial T' r.m.s. value. Radiative intensity is practically independent of time in this case.

(ii) As discussed by Kabashnikov and Kmit [34], the pro-

duct $\kappa_\nu\Lambda$ is a relevant parameter since it determines the optical thickness of a large size eddy. In the case

$$\kappa_{\nu_0}\Lambda = \frac{x_a pS(T_0)}{\pi\gamma}\Lambda \ll 1,$$

radiative intensity can again be assumed to be time independent. In addition, significant variations of the function $F(x_c)$ and its derivatives require several integral length-scales. The approximation

$$\int_0^{L_x} \frac{dF}{dx_c}(x_0)T'^2(x)\,dx \approx \theta^2 \int_0^{L_x} \frac{dF}{dx_c}(x_0)\,dx,$$

can be used and we find again one term of $(I-I(T_0))$ proportional to the sum given in (B.12).

In the opposite limit $(x_a pS(T_0)/\pi\gamma)\Lambda \gg 1$, the major contribution to radiative intensity is due to a column with a length equal to a small fraction of Λ. Intensity deviations from $I(T_0)$ result more from temporal temperature variations than spatial ones. We may expect in this case a similar behavior as that found for $\Lambda/L_x \gg 1$.